

Perceptual similarity of visual patterns predicts the similarity of their dynamic neural activation patterns measured with MEG

Susan G. Wardle¹, Nikolaus Kriegeskorte², Seyed-Mahdi Khaligh-Razavi²,
and Thomas A. Carlson^{1,*}

¹ARC Center for Cognition and its Disorders and Department of Cognitive Science, Macquarie University, Sydney, New South Wales, 2109, Australia

²Medical Research Council, Cognition and Brain Sciences Unit, Cambridge, CB2 7EF, UK

*Corresponding Author:

Thomas A. Carlson

Department of Cognitive Science

Australian Hearing Hub

16 University Avenue

Macquarie University NSW 2109 Australia

Phone : +61 2 9850 4133

Email: thomas.carlson@mq.edu.au

Acknowledgements. This research was supported by an Australian NHMRC Early Career Fellowship (APP1072245) awarded to S.G.W., a European Research Council Starting Grant (ERC-2010-StG 261352) awarded to N.K., and an Australian Research Council Future Fellowship (FT120100816) awarded to T.A.C. The authors declare no competing financial interests.

Abstract

Perceptual similarity is a cognitive judgment that represents the end-stage of a complex cascade of hierarchical processing throughout visual cortex. Although it is intuitive that visual objects that appear similar may share similar underlying patterns of neural activation, a direct mapping between perceptual similarity and representational distance has not been demonstrated. Here we explore the relationship between the human brain's time-varying representation of visual patterns and behavioral judgments of perceptual similarity. The visual stimuli were abstract patterns constructed from identical perceptual units (oriented Gabor patches) so that each pattern had a unique global form or perceptual 'Gestalt'. The visual stimuli were decodable from evoked neural activation patterns measured with magnetoencephalography (MEG), however, stimuli differed in the similarity of their neural representation as estimated by differences in decodability. Early after stimulus onset (from 50ms), a model based on retinotopic organization predicted the representational similarity of the visual stimuli. Following the peak correlation between the retinotopic model and neural data at 80ms, the neural representations quickly evolved so that retinotopy no longer provided a sufficient account of the brain's time-varying representation of the stimuli. Overall the strongest predictor of the brain's representation was a model based on human judgments of perceptual similarity, which reached the theoretical limits of the maximum correlation with the neural data defined by the 'noise ceiling'. Our results show that large-scale brain activation patterns contain a neural signature for the perceptual Gestalt of composite visual features, and demonstrate a strong correspondence between perception and complex patterns of brain activity.

Keywords: magnetoencephalography (MEG), representational similarity analysis, perceptual similarity, representational geometry, decoding, Gestalt perception

Introduction

Judgments of perceptual similarity require integrating information across a complex hierarchical network of brain regions. An early idea of how perceptual similarity might be conceived at the neural level is as a product of representational distance (Shepard, 1964; Torgerson, 1965). Specifically, visual objects that appear similar are assumed to share similar underlying neural representations. Although there has been substantial interest in revealing the transformation of representational structure across the visual processing hierarchy, a direct mapping between perceptual similarity and the similarity of brain activation patterns has not been established. Several studies have observed a correspondence between behavioral similarity judgments and neural representations; however, most of these experiments have focused on object recognition, and thus used stimuli in which perceptual similarity is unavoidably conflated with conceptual similarity (Edelman et al 1998; Mur et al 2013; Connolly et al. 2012). Other studies have emphasized the role of image statistics, and used naturalistic stimuli varying on both semantic and visual dimensions (Hiramatsu et al 2011), in which the mapping between different feature dimensions and perceptual similarity is complex.

The aim of the present study is to determine the extent to which perceptual similarity is accessible in dynamic large-scale brain activation patterns. We use two methodological advances to build on previous work: firstly, we use a novel stimulus set to decouple perceived similarity from both semantics and lower-level visual features, and secondly, we exploit the fine temporal resolution of MEG to examine the evolving representational geometry across time. To control for low-level features and semantics in the visual stimuli, we constructed visual patterns from arrangements of Gabor patches, which will drive the response of neurons in early visual cortex, and make straightforward predictions for a range of models that can be used to characterize the evoked cortical response to the stimuli. The stimulus set varied along three dimensions: the number of elements, the local orientation of each Gabor patch, and the degree of orientation coherence among the elements. Critically, although the stimuli are constructed from identical elements, each stimulus has a unique global form or perceptual 'Gestalt' (Figure 1A).

Most studies examining representational geometry have used fMRI (e.g. Clarke and Tyler, 2014; Edelman et al., 1998; Hiramatsu et al. 2011; Mur et al., 2013), and focused on the transformation of the representational space across spatial networks of brain regions. Compared to other neuroimaging methods, fMRI has limited temporal resolution, and consequently the temporal evolution of the mapping between behaviorally relevant features and the structure of neural representations has remained largely unexplored. To address this we used MEG to record time-varying patterns of brain activation in response to each visual stimulus. Thus our focus here is on the temporal (rather than spatial) evolution of the neural representational geometry in response to visual patterns.

In order to investigate the information content of the brain's time-varying representation of the stimuli, we employed representational similarity analysis (RSA; Kriegeskorte and Kievit, 2013) to test several candidate models of the representational structure. RSA is a model-testing approach for studying brain activation patterns, which builds on traditional brain 'decoding' methods (e.g. multivariate pattern analysis) to facilitate conclusions about the content of decodable information (Kriegeskorte and Kievit, 2013). The intuition behind RSA is that differences in the decodability of stimuli can be interpreted as a proxy for neural representational similarity. Stimuli that are more difficult to decode from each other are assumed to have more similar underlying neural representations. If a model successfully predicts the representational distance between stimuli, it provides evidence that the source of representational information in the model is present in the neural population code. An additional strength of applying RSA to MEG data is that the fine-scale temporal resolution of the neuromagnetic signal reveals the emergence of representational geometry over time, providing a more complete characterization of the model's performance. We recorded patterns of brain activity with MEG while participants viewed each visual stimulus. To determine whether a neural signature of global form is accessible in these neural activation patterns, we used RSA to compare models of early visual processing to a model of perceptual similarity based on human similarity judgments for the visual stimuli.

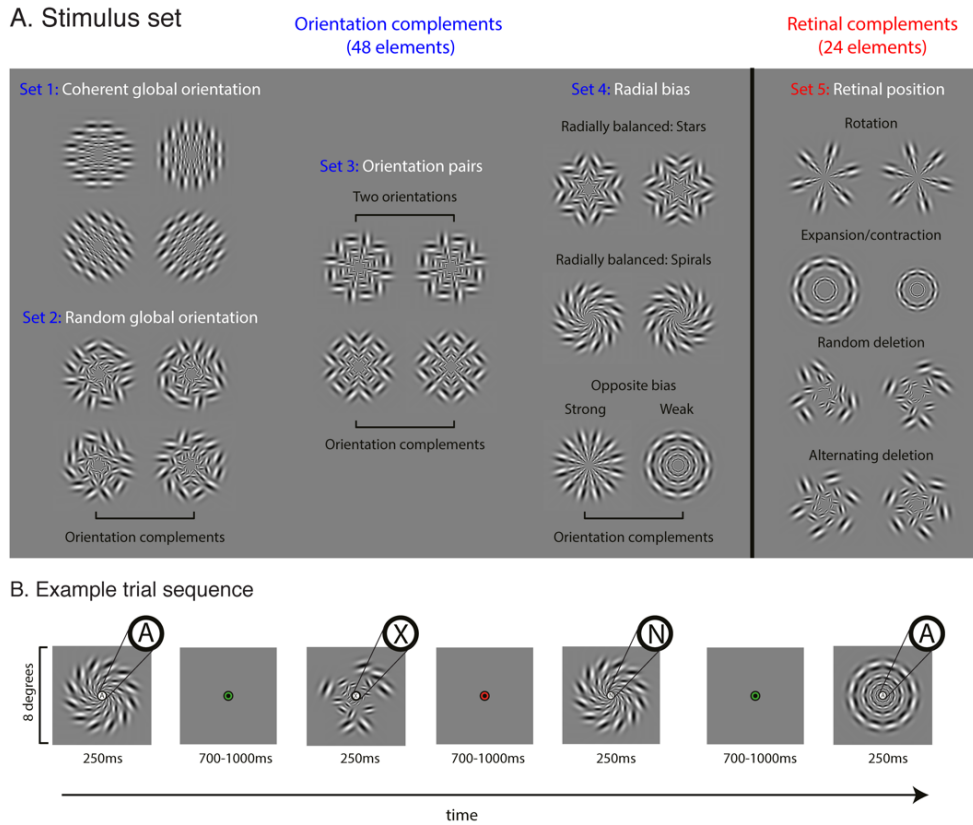


Figure 1. Experimental Design. (A) Visual stimuli in set 1 have a coherent global orientation [0° , 90° , 45° , or 135°], while the patterns in set 2 have an equivalent overall local orientation disparity but lack a coherent global orientation. Set 2 patterns were created by generating an array of elements with random orientations, and then rotating the elements of the random seed pattern by 90° , 45° , and 135° . In set 3, each pattern has alternating elements of two orientations (top pair: 0° and 90° , bottom pair: 45° and 135°), with the order of orientations swapped between the members of each pair (top and bottom rows). In set 4, the star and spiral pairs are radially balanced, with elements rotated either 45° or -45° relative to (invisible) radial spokes originating from fixation. The third pair contains one pattern with a strong radial bias (radial spokes) and one with a weak bias (rings). All pairs in set 5 are retinal complements, with the Gabor patches in complementary retinal locations.

Materials and Methods

Participants. Twenty volunteers (8 male, 12 female) with an average age of 21.6 years participated in the experiment and received financial reimbursement. Informed written consent was obtained from

each volunteer prior to the experiment, and all experimental procedures received approval from the institutional ethics committees.

Stimuli. Visual stimuli were arrays of Gabor patches (sine wave convolved with a 2D Gaussian window) in a log polar arrangement (inner radius: 1° , outer radius: 8°) with four rings and twelve spokes (Figure 1A). The size of the elements was log scaled based on their position relative to central fixation to account for cortical magnification in early visual cortex. The 26 visual stimuli were designed in 13 complementary pairs to facilitate pairwise multivariate pattern classification as a foundation for RSA. Nine stimulus pairs were *orientation* complements constructed from 48 individual Gabors (Figure 1A, sets 1-4). In each pair, elements at corresponding spatial locations were rotated 90° . These patterns were thus maximally different in terms of orientation disparity, but equivalent in terms of coarse scale retinal stimulation. The remaining four pairs were *retinal* complements, constructed from 24 individual Gabors (Figure 1A, set 5). For these pairs, elements present in one pattern were absent in the corresponding spatial location of its complement.

Procedure. Participants viewed the visual stimuli while laying supine in a magnetically shielded recording chamber. Stimuli were projected onto a translucent screen located approximately 30cm above the participant. The experiment was run on a Dell PC desktop computer using MATLAB (Natick, MA, U.S.A.) and functions from the Psychtoolbox (Brainard, 1997; Pelli, 1997; Kleiner, et al. 2007). The visual stimuli were displayed on the screen in the MEG for 250ms with a variable inter-stimulus interval (700 -1000ms). Participants ran eight blocks of trials of approximately seven minutes in length, which each contained six presentations of each visual stimulus, presented in random order (48 presentations total per stimulus). Participants performed a fixation task during the experimental runs (Figure 1B), which involved detecting whether a small letter (0.5°) in the center of the stimulus was a vowel or a consonant (randomly drawn from the set {'A' 'E' 'I' 'O' 'U' 'R' 'N' 'X' 'S' 'G'}). Feedback was provided by changing the color of the fixation target for 300ms after each trial, and a performance summary was displayed after each block of trials. The mean accuracy across participants for the task was 97% correct ($SD = 2.6\%$).

MEG Acquisition and Preprocessing. Neuromagnetic recordings were acquired with a whole-head axial gradiometer MEG system (KIT, Kanazawa, Japan). The system had 157 recording channels with 3 reference channels. Recordings were filtered online from 0.1 to 200 Hz using first order RC filters and digitized at 1000 Hz. Time shifted principal component analysis (TSPCA) was used to denoise the data offline (de Cheveigne and Simon, 2007). Trials were epoched from -100ms to 600ms relative to stimulus onset. Trials with eye movement artifacts were removed automatically using an algorithm that detects large deviations in the root mean square (RMS) amplitude over 30 selected eye-blink sensitive channels. The average rejection rate was 2.2% ($SD = 1.0\%$) of trials across participants. After artifact rejection, the data were resampled to 200Hz, and corrected for the latency offset introduced by resampling. Principle component analysis was used to reduce the dimensionality of the data. Using a criterion of retaining 99% of the variance, the number of dimensions was reduced from 157 (recording channels) to 62 principle components, on average across subjects.

Pattern Classification. We used a naïve Bayes implementation of linear discriminant analysis (LDA; Duda et al., 2001) for the decoding analysis. The input to the classifier was the factor loadings for the principle components. Generalization of the classifier was evaluated using k -fold cross validation with a ratio of 9:1 training to test. To improve the signal to noise, trials were averaged in pseudo trials (Isik et al., 2014; Meyers, 2013). Each pseudo trial was an average of four trials. The set of 48 trials per pattern (sometimes less after artifact rejection) was reduced to 10 pseudo trials by averaging a random selection of trials. Nine of the pseudo trials were used to train the classifier, and one was used to test the classifier. Thus for each pairwise comparison there were 18 trials used to train (nine from each stimulus pattern) and two used to test the classifier (one from each pattern). This procedure was repeated 100 times, each time with a new randomization. Classification accuracy is reported as average classifier performance (d -prime). The decoding analysis was run for all possible pairwise comparisons between stimulus patterns for each time point.

Model Definitions.

Within the RSA framework, we constructed several model representational dissimilarity matrices (RDMs) based on stimulus properties that may account for the decodability of the stimuli to compare

with the empirical time-varying MEG RDM. Each model makes predictions about the decodability of the visual stimuli for each pairwise stimulus comparison (exceptions noted below in model definitions). The models are not intended to be comprehensive models of neural processing, but instead are used to identify what stimulus properties may underlie their decodability from the neuromagnetic signal measured with MEG. In each case the model predictions are represented as RDMs with values normalized to range from 0 (identical in terms of the model) to 1 (extremely different in terms of the model).

Perceptual Model. Fifty participants provided ratings of the perceived similarity of the patterns in an online study conducted using Amazon's Mechanical Turk services. Participants were briefly shown (duration: ~250ms) two of the individual patterns simultaneously and rated the similarity of the patterns on a scale from 1 to 100. Each participant made ratings for all the possible pairwise comparisons (325 comparisons total), and these were used to create a perceptual representational dissimilarity matrix (RDM) for each participant. Individual RDMs were normalized to range from 0 to 1, and then averaged to create a group perceptual model RDM (Figure 3B).

Retinal Envelope Model. Previously, we have shown that differences in retinal projection between higher-level object stimuli are a robust predictor of their decodability with MEG (Carlson et al., 2011). To evaluate the role of retinal projection in the representational geometry of the current lower-level visual stimuli we constructed a model that predicts decodability based solely on differences between exemplars in terms of coarse scale retinotopic stimulation (Figure 3B). Specifically, this model predicts that pairs of stimuli which have individual Gabors in *different* spatial locations (retinal positions relative to central fixation) relative to each other (e.g. Figure 1, pairs in Set 5) will be easier to decode than pairs that have individual Gabor elements in spatially corresponding locations (e.g. Figure 1, Sets 1-4). Thus the retinal envelope model predicts decodability solely on the basis of differences in local retinal position between stimulus pairs. To compute dissimilarity of their retinal position, each element location in the stimulus is a location in a vector; and at each location in the vector a 1 or 0 indicates the presence or absence of a Gabor patch. The dissimilarity between two stimulus patterns is the absolute difference between the two patterns' vectors. Dissimilarity was computed for all possible pairwise comparisons between the patterns to create the model RDM.

V1 Model (HMAX-S1). To approximate the response of early visual areas to the stimuli, we employed the HMAX model. The S1 layer of HMAX encodes orientation at multiple scales, based on

knowledge of receptive field properties of neurons in early visual areas (Riesenhuber and Poggio, 1999; Serre and Riesenhuber 2004; Hubel and Weisel, 1965). The dissimilarity between the visual stimuli for HMAX's S1 layers was computed using code available on the web (<http://cbcl.mit.edu/jmutch/cns/index.html#hmax>). The inputs to HMAX were the images of the visual stimuli (rendered at 600 x 600 pixel resolution). HMAX returns a feature vector, which represents the simulated cortical response to the stimulus. To compute dissimilarity between the stimuli, we computed the Euclidean distance between the feature vectors for each stimulus pair. Dissimilarity was computed for all possible pairwise comparisons between the stimuli to create the V1 model RDM (Figure 3B).

Orientation Disparity model. The orientation disparity model predicts decodability based on local orientation differences between the stimuli (Figure 4A). Orientation disparity was computed by summing the absolute orientation difference between corresponding Gabor elements in each stimulus pair. Dissimilarity was computed for all possible pairwise comparisons between the stimuli and then normalized to create the model RDM. Note that this model only makes predictions for the decodability of patterns with all of the 48 elements (Figure 1, Sets 1-4), as it is not possible to compute orientation disparity for unpaired Gabor patches.

Radial Preference model. Neurophysiological studies have observed a bias in the number of neurons representing radial orientations (i.e. orientations that point toward the fovea; LeVick and Thibos, 1982; Leventhal and Schall, 1983; Schall et al., 1986), and this bias has also been observed in human fMRI studies (Sasaki et al., 2006; Mannion et al., 2010; Alink et al., 2013). The radial preference model predicts decodability based on inter-stimulus differences in the radial bias (Figure 4A). We modeled the radial bias in the stimuli by computing each element's orientation disparity relative to the radial orientation for its location in the visual pattern relative to fixation (θ), and taking its cosine (e.g. 0° disparity = 1, 90° disparity = 0). The difference in the radial bias between two patterns was calculated as the sum of the absolute value of the difference between the radial bias responses for their spatially corresponding Gabor elements. Note that this model also only makes predictions for the decodability of patterns with all of the 48 elements (Figure 1, Sets 1-4).

RSA Model Evaluation. We used the RSA framework (Kriegeskorte et al., 2008; Nili, et al., 2014) to study the brain's emerging representation of the stimuli by comparing the models to time resolved MEG RDMs (Cichy et al., 2014; Redcay and Carlson, 2014). Correspondence between the empirical

RDM (MEG data) and the normalized model RDMs was assessed by computing Kendall's tau-a (i.e., a rank-order correlation) for each time point and each subject, producing a time-varying correlation between the model and MEG data. Significance was assessed with a non-parametric Wilcoxon signed rank test (FDR < 0.05). A cluster threshold of 3 consecutive time points was used to determine onset latencies.

We used the 'noise ceiling' as a benchmark for model performance (Nili, et al., 2014). The noise ceiling estimates the magnitude of the expected correlation between the true model RDM and the MEG RDM given the noise in the data. The upper bound is calculated by correlating the group average MEG RDM with the individual RDMs. This correlation is overfitted to the individual RDMs and produces an upper estimate of the true model's average correlation. The lower bound is calculated by the 'leave-one-subject-out' approach, so that each subject's individual RDM is correlated with the RDM for all remaining subjects, preventing overfitting. The average correlation across all iterations of this calculation underestimates the correlation with the true model and defines the lower bound of the expected correlation with the true model RDM.

Results

Early Decoding of Abstract Visual Patterns from MEG

Recent MEG decoding studies have shown that early visual feature representations (e.g., retinotopic location, orientation, and spatial frequency) and higher-level object categories can be decoded from neuromagnetic recordings (Carlson, et al. 2011; Carlson et al., 2013; Cichy et al., 2014; Ramkumar, et al. 2013). We first examined whether it was possible to decode the abstract patterns (Figure 1A). Decoding analysis was performed using a naïve Bayes implementation of linear discriminant analysis (LDA, Duda et al. 2001), in which the classifier was trained to decode the visual stimulus that a participant was viewing from the corresponding MEG recordings. The decoding analysis was run for all possible pairwise comparisons between visual stimuli for each time point. Figure 2 shows average decoding performance as a function of time. Classification accuracy, reported as d -prime, is the average classifier performance. Decoding performance is above chance beginning 40ms after stimulus onset, consistent with estimates of the latency of visual inputs to reach the cortex (Aine, Supek, and George, 1995; Jeffreys and Axford, 1972; Nakamura et al., 1997; Supek et al., 1999), and with the

onset of spatial frequency (51ms) and orientation decoding (65ms) from MEG (Ramkumar et al., 2013). After onset, decoding performance rises to a peak at 90ms and then decays slowly. Following the initial peak at 90ms, there is a second smaller peak in decoding at 400ms, which corresponds to stimulus offset (Carlson, et al. 2011).

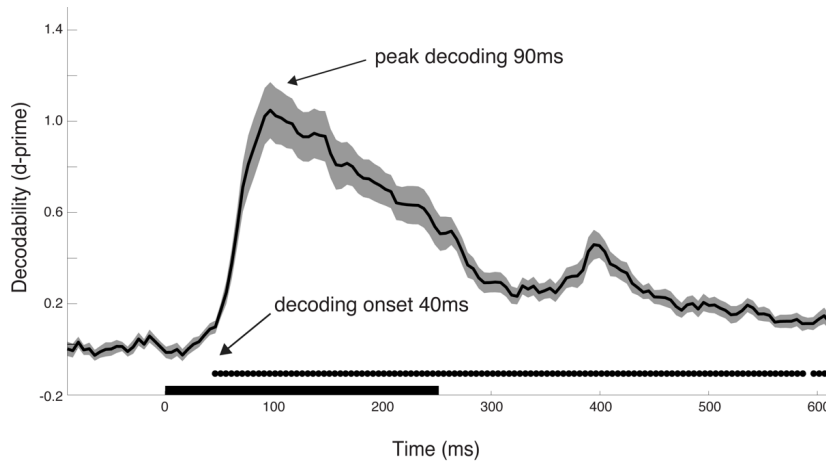
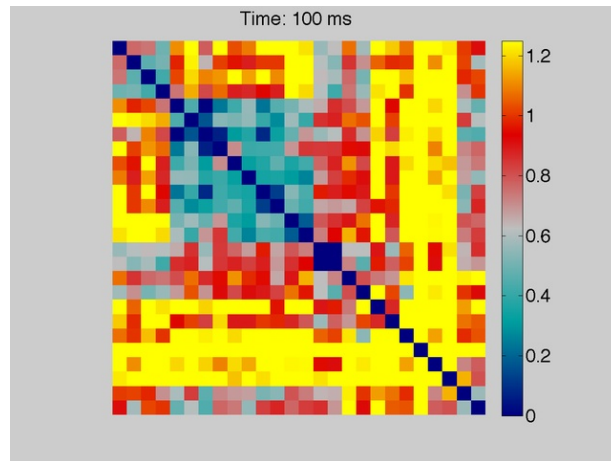


Figure 2. Decodability of the Visual Stimuli. Solid line is classifier performance (d -prime) averaged across all subjects ($N=20$) and stimulus pairs ($N=325$) as a function of time. The black bar on the x-axis corresponds to stimulus presentation. Shaded region marks ± 1 S.E.M. Disks below the plot indicate above chance decoding performance (onset at 40ms), with significance evaluated using a Wilcoxon signed rank test (FDR < 0.05).

Perceived Similarity Predicts Decodability

The capacity to decode the visual stimuli from patterns of neural activation shows that information related to the visual stimuli exists in the MEG signal. We then used RSA to investigate the nature of this decodable signal. We first constructed an empirical RDM for each time point from the pairwise decoding performance, which represents the decodability of the neural patterns associated with visual stimulation as a function of time. The time-varying RDM (Movie 1) shows a detailed representation of the averaged data plotted in Figure 2, as the decodability of each pairwise comparison is shown evolving over time with millisecond resolution. To summarize the overall decodability of the stimulus set, we calculated the time-averaged RDM from the first time point in which decodability is above

chance (40ms) to stimulus offset (250ms). The average RDM (Figure 3A) quantifies how decodable each unique stimulus pair is and measures the similarity between their neural activation patterns. There is clear visible structure in the RDM, indicating that some stimuli share a more similar neural representation than others. The time-averaged RDM in Figure 3A is for illustration, for the formal model comparisons we used the complete time-varying RDM (Movie 1).



Movie 1. Time-varying representational dissimilarity matrix (RDM) for all pairwise stimulus comparisons. The movie shows the mean decodability (d' -prime) of all stimulus pairs from the MEG data as a function of time (5 ms resolution) from 50 ms before stimulus onset to 605 ms after stimulus onset. The 90 ms frame of the movie corresponds to the peak decoding at 90ms shown in Figure 2, and is dominated by warm colors in the RDM, indicating a high level of decodability for most stimulus pairs. The order of the stimulus pairs along the axes is identical to that shown in Figure 3A. [*author note: movie file is not available in the electronic preprint version of this article*].

Our central question is how perceived similarity relates to the brain's emerging representation of the stimuli. We addressed this within the RSA framework by constructing a perceptual model that predicts the relative decodability of each stimulus pair based on perceived similarity as rated by human observers. The perceptual model RDM is the average of the normalized ratings for each pair made by each observer (Figure 3B). The perceptual model RDM (Figure 3B) shows clear structure, indicating that stimulus pairs varied in their perceived similarity. In order to assess the correspondence between

the perceptual model and the MEG data, we used a rank-order correlation (Kendall's tau a) between the model and empirical RDMs across time (Figure 3E). Significant correspondence between the model and the data was assessed with a non-parametric Wilcoxon signed rank test.

We observed a strong correspondence between the behavioral ratings of perceived similarity made by human observers and the brain's time-varying representation of the stimuli, which is evident by visual inspection of the neural and behavioral RDMs (compare Figure 3A to the perceptual model in Figure 3B). This correspondence is supported by a significant time-varying correlation between the perceptual model and decodability (black trace, Figure 3C). The correlation between the model predictions and the decodability of the patterns begins 50ms after stimulus onset, and remains significant over almost the entire time interval. In addition, the correlation between the neural data and perceptual model closely tracks the lower bound of the noise ceiling from approximately 150ms after stimulus onset (black dotted line in Figure 3C). This shows that the magnitude of the observed correlation between the behavioral and neural RDMs is within the theoretical upper limits for the data, thus the perceptual model provides an explanation of the data comparable with the true (unknown) model (Nili et al, 2014).

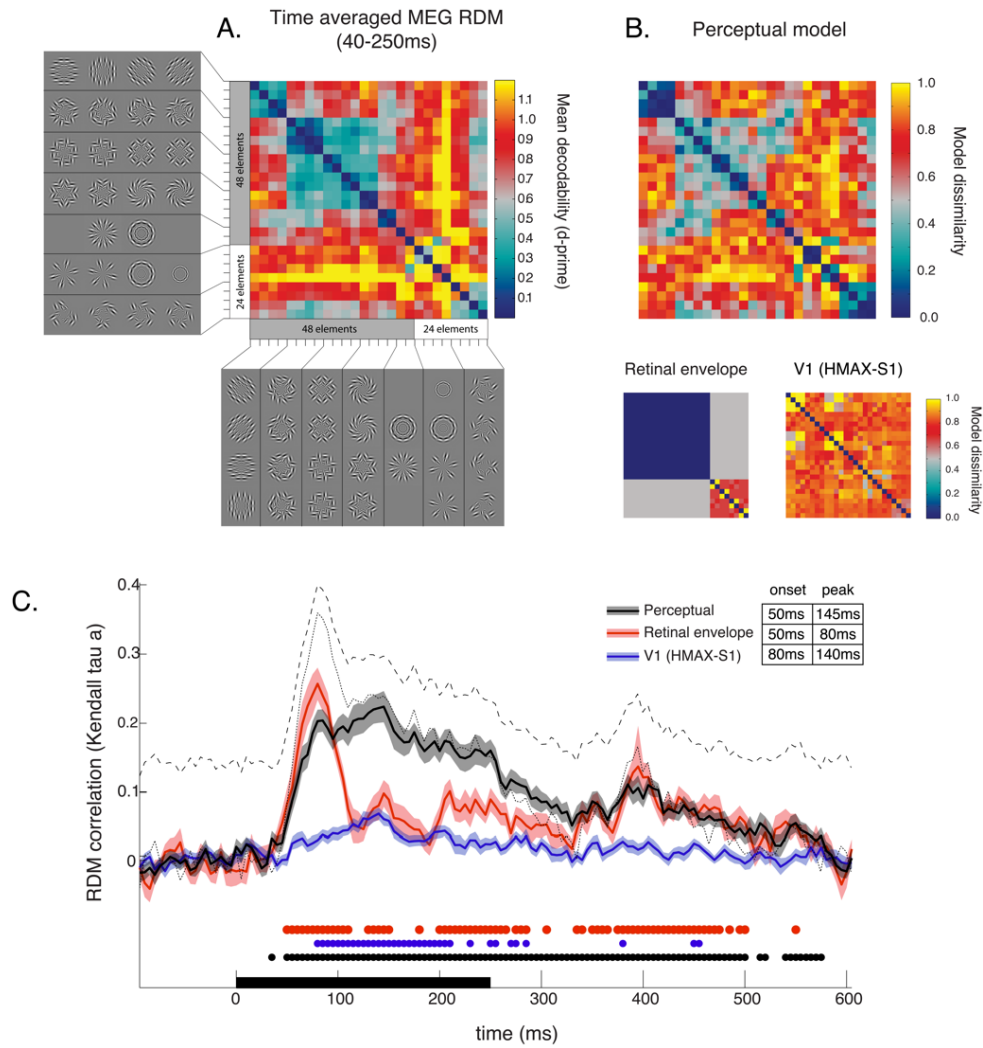


Figure 3. RDM Model Comparisons. (A) Empirical RDM displaying the time-averaged decodability of all exemplar pairings from the time decodability first is above chance (40ms) to stimulus offset (250ms). (B) Model RDMs scaled to range from 0 (identical) to 1 (highly dissimilar) for the perceptual similarity model, the retinal envelope model, and the V1 model. (C) Colored lines are time-varying correlations between model predictions and MEG decoding performance averaged across subjects (shaded region: ± 1 SEM). Dashed and dotted lines represent the 'noise ceiling', (Nili, et al., 2014). Colored disks below each plot indicate a significant correlation, evaluated using a Wilcoxon signed rank test (FDR < 0.05). The black bar on the x-axis indicates the stimulus duration.

Can Early Visual Representations Explain Decodability?

Perceptual similarity proved to be a near-optimal model for predicting the neural similarity between abstract visual patterns. For comparison we tested additional models of low-level visual features and early visual processing that we reasoned were likely to predict decodability. First, we constructed a retinal envelope model that predicts decodability based on inter-stimulus differences in retinal projection, as we have previously observed that retinal projection predicts the decodability of higher-level object stimuli from MEG (Carlson et al., 2011). The retinal envelope model (Figure 3B) significantly correlates with the MEG RDM beginning 50ms after stimulus onset (Figure 3C). Following this early onset, the model correlation peaks at 80ms and then declines sharply. The early success of this model indicates that the difference between the retinotopic projections of stimuli is an important factor in the similarity of their neural representation at the large-scale pattern level, particularly immediately after stimulus onset. The model, however, fails to capture the complex structure of the neural representation of the stimuli (Figure 3A), and following this sharp early peak at 80ms (which is well below the theoretical maximum defined by the noise ceiling), the model's predictive power drops quickly.

While retinotopic organization is clearly a dominant organizational principle in visual cortex, early visual areas also encode a range of visual features, e.g. orientation, that are not present in the retinal envelope model. Orientation selectivity is evident in the earliest stages of visual processing and is encoded in simple cell neurons in visual cortex (Hubel and Wiesel, 1962, 1968). To construct a more complete model of early visual processing, we built a model based on the response properties of V1 simple cells from the predicted response profiles to the visual stimuli from the output of the S1 layer of HMAX, a computational model of early visual processing, which represents orientation at multiple scales (Riesenhuber and Poggio, 1999; Serre and Riesenhuber 2004; Hubel and Weisel, 1965). The V1-HMAX model in Figure 3B predicts that nearly all stimulus pairs will be highly decodable. The model did fit the MEG data beginning from 80ms, with a peak at 140ms. However, the V1-HMAX model did not approximate the noise ceiling at any latency, and was not as strong a predictor of the neural data as either the perceptual model or the retinal envelope model. Additional “higher” layers of HMAX up to layer C2 were also tested and performed similarly (Figure 4). Each layer of HMAX first reached a significant correlation with the empirical MEG RDM between 55-90ms, and for some sporadic time

points thereafter, but overall none of the HMAX layers was a strong predictor of the MEG data.

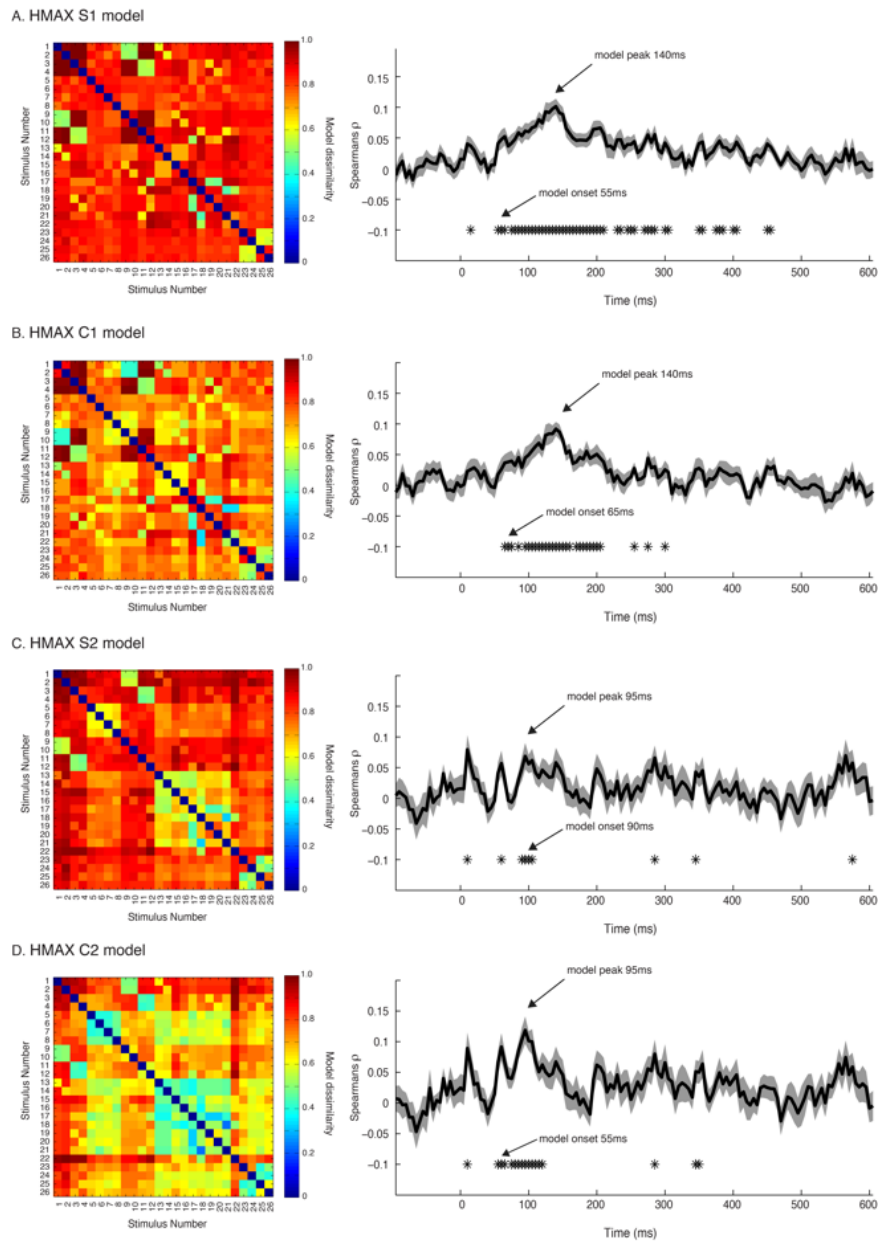


Figure 4. Average decodability across four layers of HMAX. Each row A-D shows the model predictions (left panel) and the time-varying correlation between the model and the MEG data (right panel) separately for a level of HMAX (S1, C1, S2, C2). Panels on the left show the model RDM's for the four HMAX layers. Color values in the RDM represent the dissimilarity between the pairs of patterns as predicted by the assumptions of each model layer. Panels on the right show the model correlation with MEG decoding performance. Plotted is the Spearman rank-order correlation between the model RDM and the time-varying MEG decoding RDMs. The solid line is the average correlation

across subjects. The shaded region is ± 1 S.E.M. Asterisks below the plot indicate a significant correlation, evaluated using a Wilcoxon signed rank test (FDR < 0.05).

We speculated that one reason for the limited explanatory power of the V1 model based on HMAX is possibly because it assigns too high a weight to local orientation differences between the stimuli, and fails to capture the perceptually salient differences in global form, which are highly weighted by the perceptual model. To verify that local orientation differences are a poor predictor of decodability, we constructed a RDM based on the overall magnitude of the orientation disparity between corresponding elements in the stimulus pairs (Figure 5A). Although this model was unsuccessful at predicting the neural data at any time point (Figure 5A), we found that we could decode the orientation of the stimulus pairs that had a coherent global orientation (Figure 5B, blue trace; Figure 1, Set 1), consistent with previous reports of orientation decoding with MEG (Duncan et al, 2010; Ramkumar, et al. 2013). Analogous to fMRI results (Alink et al., 2013), decoding was moderated by orientation coherence among the elements, because stimulus pairs with an equivalent local disparity but an absence of a coherent global orientation could not be decoded (Figure 5B, green trace; Figure 1, Set 2). This suggests that grouping across local elements is a strong component of the underlying neural representation.

Orientation decoding with fMRI has been suggested to be a byproduct of the radial bias – the greater number of neurons representing orientations pointing toward the fovea (Levick and Thibos, 1982; Leventhal and Schall, 1983; Schall et al., 1986; Sasaki et al., 2006; Mannion et al., 2010), however, this issue remains controversial (e.g. Carlson, 2014; Freeman et al., 2011; Freeman et al., 2013; Mannion et al., 2009; Alink et al., 2013; Maloney, 2015; Clifford and Mannion, 2015; Carlson and Wardle, 2015). We found that a RDM modeled on inter-stimulus differences in the radial bias did not fit the MEG data; the radial preference model never reached significance at any time point (Figure 5A). In addition, we found that decoding of stimulus pairs designed to test for radial bias effects was instead moderated by differences in their global form. Stimuli that were matched for the magnitude of the radial bias that had similar global form (within-shape decoding of stars or spirals; see radially balanced pairs in Figure 1, Set 4) could not be decoded (Figure 5C, green trace). However, these radially-balanced stimuli could be decoded in between-shape pairs (ie: across shape decoding of stars versus

spirals) in which they differed in global form (Figure 5C, blue trace). Furthermore, decoding performance for the stimulus pair that was maximally different with respect to the radial bias (strong [spokes] versus weak [rings], see final pair in Set 4, Figure 1) was not substantially better than the pair that were radially balanced but differed in global form (Figure 5C, black trace). In sum, the orientation and radial bias results may be interpreted as additional support for the importance of global form in the neural representation.

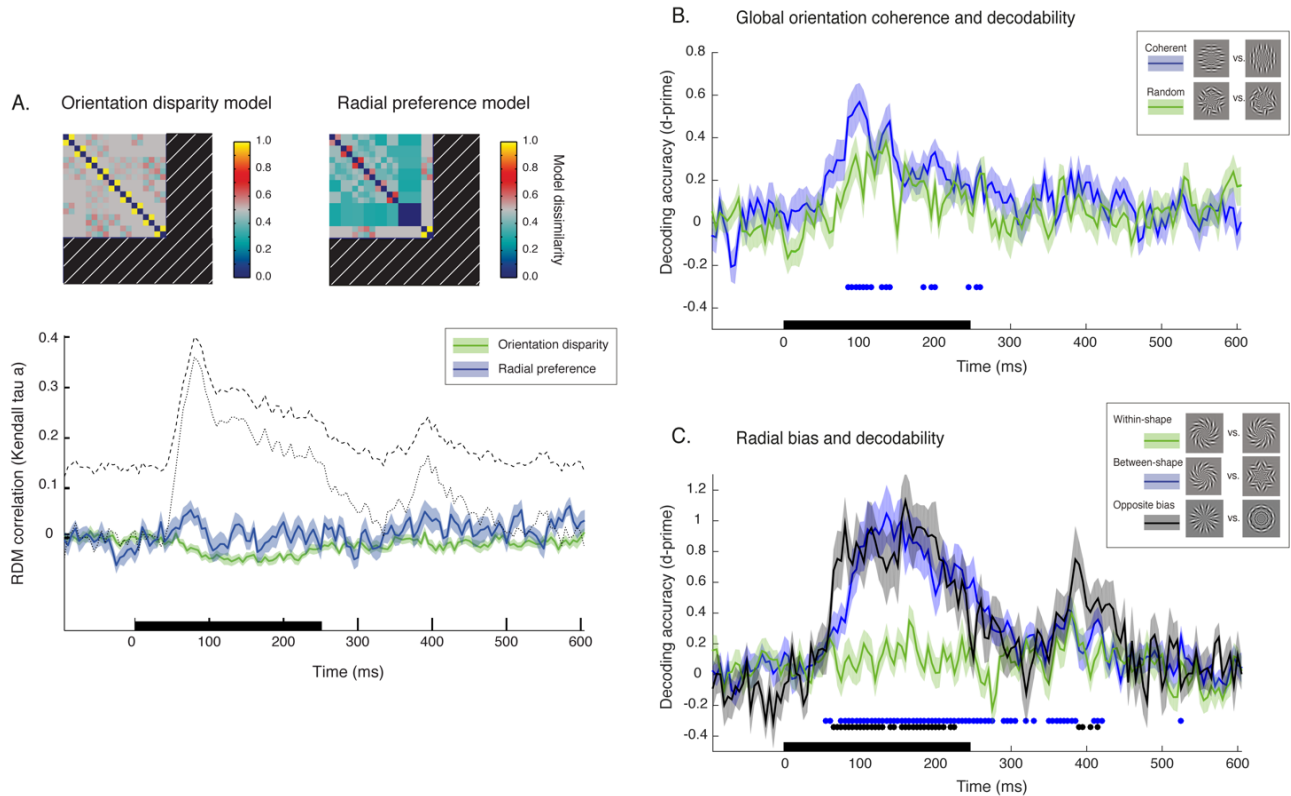


Figure 5. Orientation and the radial bias. (A) Top: Model RDMs for orientation disparity and radial preference. Hatched regions mark the undefined predictions for each model; both orientation disparity and radial preference were only calculated for the patterns with all 48 elements in corresponding retinal locations. Bottom: Correlation between model RSMs and the MEG RDM (details as in Figure 3C). (B) Orientation: Average decodability for all pairwise comparisons ($n=6$) between the four patterns that have a coherent global orientation (blue trace), and average decodability ($n=6$) for the four 'random' patterns which have equivalent local orientation disparity without coherent global orientation (green trace). (C) Radial bias: Average decoding accuracy for the two radially balanced pairs of the same shape (green trace); average decoding accuracy for the four possible between-shape pairs (blue trace);

and decodability for the stimuli differing in the strength of the radial bias (black trace). Errors are ± 1 SEM.

Discussion

Our main finding is that the perceived similarity of visual patterns predicts their representational similarity in large-scale neural activation patterns measured with MEG. We observed that perceptual similarity ratings reached the theoretical limits of the highest possible correlation with the representational structure measured with MEG from just 150ms after stimulus onset, and the success of the model persisted for several hundred milliseconds beyond stimulus offset. This demonstrates that differences in perceived global form are matched by equivalent differences in neural representational distance. As previous studies using RSA to compare neural data to behavioral models have not used an estimate of goodness-of-fit, it is not possible to directly compare the relative success of models across studies, however, we are the first to our knowledge to demonstrate a model within the RSA framework which falls within the ‘noise ceiling’ (Nili et al, 2014). This indicates that the perceptual model explained as much of the variability in the similarity of the brain activation patterns elicited by the visual stimuli as the unknown true model.

The strong correlation we observed between behavior and neural representation is a reflection of our stimulus set, which was designed to probe the neural representation of global form while controlling for low-level visual features. As all stimuli were constructed from identical visual features (Gabor patches), we assume that observers based their similarity judgments on the overall global form or Gestalt of each pattern created by the particular arrangement of Gabor patches. The fact that global form is the most salient difference between our stimuli is also consistent with the relatively poor performance of the V1 model based on HMAX. We suggest that the poor performance of the V1 model is likely because it weights local orientation differences highly while ignoring global form, and local orientation differences were a poor predictor of decodability. The best performing model assessed using RSA is always relative to the stimulus set, thus in order to demonstrate a tight link between perceptual similarity and neural activation patterns, it is necessary to use stimuli in which differences in global form are separated from both semantic similarity and low level visual parameters.

Similarly, Mur et al. (2013) used RSA and found that human similarity judgments for higher-level object stimuli did show similarity with categorical divisions in representational structure in IT; however, in this case the similarity judgments contained additional structure not present in the neural representation. The human judgments showed a tighter categorical clustering than the fMRI data, and contained a finer grain of categorical distinctions. In the Mur et al. (2013) study, similarity judgments were likely based on both semantic and visual characteristics, as the stimuli were pictures of objects, which have inherent conceptual meaning. The visual stimuli we used were abstract, thus we assume observers' similarity judgments were based solely on perceived visual similarity.

We have shown that human perceptual similarity ratings for abstract visual patterns have a strong correspondence with the underlying representational geometry. The behavioral data was collected from a separate group of subjects than the MEG data, and involved a relatively coarse judgment of similarity for each pair of stimuli on a scale from 1 to 100. The use of separate subjects for neural and behavioural data collection is common in RSA studies, and a strength of the RSA approach is its ability to examine representational structure across different subjects and methodologies. We have shown that it is possible for a behavioral RSA model to reach the theoretical limits of the best possible account of the neural representation, and future work will determine whether this can be achieved at finer scales (for example, fine perceptual discriminations). A further implication of the success of the behavioral data in predicting the neural representation (from a separate pool of subjects) is that it provides empirical validation of the common assumption that the structure of brain representations can be inferred from behavioral research. Individually the behavioral and MEG study would have reached the same conclusion; however, the bridging of the two studies using the RSA framework strengthens the conclusion and validates each approach (behavior and neuroimaging).

Our finding that whole-brain activation patterns reflect perceptually important features is consistent with recent neurophysiological and neuroimaging studies suggesting that the representation of visual inputs changes throughout the visual stream. These studies have shown that the representation in early visual areas reflects low-level visual features such as image statistics (Clarke and Tyler, 2014; Hiramatsu, et al 2011). In higher visual brain regions, the representation is instead based on higher-level features such as object category membership (Edelman et al., 1998; Clarke and Tyler, 2014) or

shape similarity (Op de Beek et al., 2001). Furthermore, differences in image statistics are diagnostic of the degree of dissimilarity of large-scale activation patterns measured with EEG (Groen et al., 2012). The early success of the retinal envelope model in predicting the decodability of our stimuli (peak performance just 80ms after stimulus onset) is consistent with the dominance of early visual features in the representational structure directly after stimulus onset, which later evolves into a representation highly correlated with perceptual similarity.

Conclusions

We found that visual stimuli that were perceived to look more similar to each other by human observers also had more similar complex neural activation patterns as measured with MEG. The behavioral model was a near-optimal predictor of neural representational similarity, and closely tracked the theoretical limits of the maximum possible correlation with the neural data from just 150 ms post-stimulus onset. We are the first to our knowledge to demonstrate a model within the RSA framework that reaches the theoretical limits of the best possible fit to the neural data as defined by the ‘noise ceiling’ (Nili et al, 2014). The results are significant because they show that the perceptual Gestalt of an image is captured in coarse-scale neuromagnetic activation patterns, and thus provide evidence that perceived similarity can indeed be conceptualized as representational distance. The decodable MEG signal emerges from complex neural activity at multiple scales throughout the visual processing hierarchy, and it is both remarkable and logical that the geometry of this pooled neural activity represents an end-stage as advanced as human judgments of perceived similarity.

References

- Aine, C. J., Supek, S., & George, J. S. (1995). Temporal dynamics of visual-evoked neuromagnetic sources: effects of stimulus parameters and selective attention. *The International Journal of Neuroscience*, *80*(1-4), 79–104.
- Alink, A., Krugliak, A., Walther, A., & Kriegeskorte, N. (2013). fMRI orientation decoding in V1 does not require global maps or globally coherent orientation stimuli. *Frontiers in Psychology*, 1–14. doi:10.3389/fpsyg.2013.00493/abstract
- Brainard, D. (1997). The Psychophysics Toolbox. *Spatial Vision*, *10*(4), 433–436.
- Carlson, T. A. (2014). Orientation decoding in human visual cortex: new insights from an unbiased perspective. *The Journal of Neuroscience*, *34*(24), 8373–8383. doi:10.1523/JNEUROSCI.0548-14.2014
- Carlson, T. A., & Wardle, S. G. (2015). Sensible decoding. *NeuroImage*, *110*(C), 217–218. doi:10.1016/j.neuroimage.2015.02.009
- Carlson, T. A., Hogendoorn, H., Kanai, R., Mesik, J., & Turret, J. (2011). High temporal resolution decoding of object position and category. *Journal of Vision*, *11*(10), 9–9. doi:10.1167/11.10.9
- Carlson, T., Tovar, D. A., Alink, A., & Kriegeskorte, N. (2013). Representational dynamics of object vision: the first 1000 ms. *Journal of Vision*, *13*(10), 1–1. doi:10.1167/13.10.1
- Cichy, R. M., Pantazis, D., & Oliva, A. (2014). Resolving human object recognition in space and time. *Nature Neuroscience*, *17*(3), 455–462. doi:10.1038/nn.3635
- Clarke, A., & Tyler, L. K. (2014). Object-specific semantic coding in human perirhinal cortex. *The Journal of Neuroscience*, *34*(14), 4766–4775. doi:10.1523/JNEUROSCI.2828-13.2014
- Clifford, C. W. G., & Mannon, D. J. (2015). Orientation decoding: Sense in spirals? *NeuroImage*, *110*, 219–222. doi:10.1016/j.neuroimage.2014.12.055
- Connolly, A. C., Guntupalli, J. S., Gors, J., Hanke, M., Halchenko, Y. O., Wu, Y.-C., et al. (2012). The representation of biological classes in the human brain. *The Journal of Neuroscience*, *32*(8), 2608–2618. doi:10.1523/JNEUROSCI.5547-11.2012
- de Cheveigné, A., & Simon, J. Z. (2007). Denoising based on time-shift PCA. *Journal of Neuroscience Methods*, *165*(2), 297–305. doi:10.1016/j.jneumeth.2007.06.003
- Duda, R. O., Hart, P. E., & Stork, D. G. (2001). *Pattern classification* (2nd ed.). New York, NY:

Wiley.

- Duncan, K. K., Hadjipapas, A., Li, S., Kourtzi, Z., Bagshaw, A., & Barnes, G. (2010). Identifying spatially overlapping local cortical networks with MEG. *Human Brain Mapping, 31*(7), 1003–1016. doi:10.1002/hbm.20912
- Edelman, S., Grill-Spector, K., Kushnir, T., & Malach, R. (1998). Toward direct visualization of the internal shape representation space by fMRI. *Psychobiology, 26*(4), 309–321. doi:10.3758/BF03330618
- Freeman, J., Brouwer, G. J., Heeger, D. J., & Merriam, E. P. (2011). Orientation decoding depends on maps, not columns. *The Journal of Neuroscience, 31*(13), 4792–4804. doi:10.1523/JNEUROSCI.5160-10.2011
- Freeman, J., Heeger, D. J., & Merriam, E. P. (2013). Coarse-scale biases for spirals and orientation in human visual cortex. *The Journal of Neuroscience, 33*(50), 19695–19703. doi:10.1523/JNEUROSCI.0889-13.2013
- Groen, I. I. A., Ghebreab, S., Lamme, V. A. F., & Scholte, H. S. (2012). Spatially Pooled Contrast Responses Predict Neural and Perceptual Similarity of Naturalistic Image Categories. *PLoS Computational Biology, 8*(10). doi:10.1371/journal.pcbi.1002726
- Hiramatsu, C., Goda, N., & Komatsu, H. (2011). Transformation from image-based to perceptual representation of materials along the human ventral visual pathway. *NeuroImage, 57*(2), 482–494. doi:10.1016/j.neuroimage.2011.04.056
- Hubel, D. H., & Wiesel, T. N. (1962). Receptive fields, binocular interaction and functional architecture in the cat's visual cortex. *The Journal of Physiology, 160*, 106–154.
- Hubel, D. H., & Wiesel, T. N. (1965). Receptive fields and functional architecture in two nonstriate visual areas (18 and 19) of the cat. *Journal of Neurophysiology, 28*, 229–289.
- Hubel, D. H., & Wiesel, T. N. (1968). Receptive fields and functional architecture of monkey striate cortex. *The Journal of Physiology, 195*(1), 215–243.
- Isik, L., Meyers, E. M., Leibo, J. Z., & Poggio, T. (2014). The dynamics of invariant object recognition in the human visual system. *Journal of Neurophysiology, 111*(1), 91–102. doi:10.1152/jn.00394.2013
- Jeffreys, D. A., & Axford, J. G. (1972). Source locations of pattern-specific components of human visual evoked potentials. I. Component of striate cortical origin. *Experimental Brain Research,*

16(1), 1–21.

- Kleiner, M., Brainard, D., & Pelli, D. (2007). What's new in Psychtoolbox-3? *Perception*, 36 (ECPV Abstract Supplement).
- Kriegeskorte, N., & Kievit, R. A. (2013). Representational geometry: integrating cognition, computation, and the brain. *Trends in Cognitive Sciences*, 17(8), 401–412.
doi:10.1016/j.tics.2013.06.007
- Kriegeskorte, N., Mur, M., & Bandettini, P. (2008). Representational similarity analysis - connecting the branches of systems neuroscience. *Frontiers in Systems Neuroscience*, 2, 4.
doi:10.3389/neuro.06.004.2008
- Leventhal, A. G., & Schall, J. D. (1983). Structural basis of orientation sensitivity of cat retinal ganglion cells. *The Journal of Comparative Neurology*, 220(4), 465–475.
doi:10.1002/cne.902200408
- Levick, W. R., & Thibos, L. N. (1982). Analysis of orientation bias in cat retina. *The Journal of Physiology*, 329, 243–261.
- Maloney, R. T. (2015). The basis of orientation decoding in human primary visual cortex: fine- or coarse-scale biases? *Journal of Neurophysiology*, 113(1), 1–3. doi:10.1152/jn.00196.2014
- Mannion, D. J., McDonald, J. S., & Clifford, C. W. G. (2009). Discrimination of the local orientation structure of spiral Glass patterns early in human visual cortex. *NeuroImage*, 46(2), 511–515.
doi:10.1016/j.neuroimage.2009.01.052
- Mannion, D. J., McDonald, J. S., & Clifford, C. W. G. (2010). Orientation anisotropies in human visual cortex. *Journal of Neurophysiology*, 103(6), 3465–3471. doi:10.1152/jn.00190.2010
- Meyers, E. M. (2013). The neural decoding toolbox. *Frontiers in Neuroinformatics*, 7, 8.
doi:10.3389/fninf.2013.00008
- Mur, M., Meys, M., Bodurka, J., Goebel, R., Bandettini, P. A., & Kriegeskorte, N. (2013). Human Object-Similarity Judgments Reflect and Transcend the Primate-IT Object Representation. *Frontiers in Psychology*, 4, 128. doi:10.3389/fpsyg.2013.00128
- Nakamura, A., Kakigi, R., Hoshiyama, M., Koyama, S., Kitamura, Y., & Shimojo, M. (1997). Visual evoked cortical magnetic fields to pattern reversal stimulation. *Cognitive Brain Research*, 6(1), 9–22.
- Nili, H., Wingfield, C., Walther, A., Su, L., Marslen-Wilson, W., & Kriegeskorte, N. (2014). A toolbox

- for representational similarity analysis. *PLoS Computational Biology*, *10*(4), e1003553.
doi:10.1371/journal.pcbi.1003553
- Op de Beeck, H., Wagemans, J., & Vogels, R. (2001). Inferotemporal neurons represent low-dimensional configurations of parameterized shapes. *Nature Neuroscience*, *4*(12), 1244–1252.
doi:10.1038/nn767
- Pelli, D. G. (1997). The VideoToolbox software for visual psychophysics: transforming numbers into movies. *Spatial Vision*, *10*(4), 437–442.
- Ramkumar, P., Jas, M., Pannasch, S., Hari, R., & Parkkonen, L. (2013). Feature-specific information processing precedes concerted activation in human visual cortex. *The Journal of Neuroscience*, *33*(18), 7691–7699. doi:10.1523/JNEUROSCI.3905-12.2013
- Redcay, E., & Carlson, T. A. (2015). Rapid neural discrimination of communicative gestures. *Social Cognitive and Affective Neuroscience*, *10*(4), 545–551. <http://doi.org/10.1093/scan/nsu089>
- Riesenhuber, M., & Poggio, T. (1999). Hierarchical models of object recognition in cortex. *Nature Neuroscience*, *2*(11), 1019–1025. doi:10.1038/14819
- Sasaki, Y., Rajimehr, R., Kim, B. W., Ekstrom, L. B., Vanduffel, W., & Tootell, R. B. H. (2006). The radial bias: a different slant on visual orientation sensitivity in human and nonhuman primates. *Neuron*, *51*(5), 661–670. doi:10.1016/j.neuron.2006.07.021
- Schall, J. D., Perry, V. H., & Leventhal, A. G. (1986). Retinal ganglion cell dendritic fields in old-world monkeys are oriented radially. *Brain Research*, *368*(1), 18–23.
- Serre, T., & Riesenhuber, M. (2004). Realistic Modeling of Simple and Complex Cell Tuning in the HMAX Model, and Implications for Invariant Object Recognition in Cortex. Technical Report CBCL Paper 239 / AI Memo 2004-017, Massachusetts Institute of Technology, Cambridge, MA, July 2004.
- Shepard, R. N. (1964). Attention and the metric structure of the stimulus space. *Journal of Mathematical Psychology*, *1*(1), 54–87. doi:10.1016/0022-2496(64)90017-3
- Supek, S., Aine, C. J., Ranken, D., Best, E., Flynn, E. R., & Wood, C. C. (1999). Single vs. paired visual stimulation: superposition of early neuromagnetic responses and retinotopy in extrastriate cortex in humans. *Brain Research*, *830*(1), 43–55.
- Torgerson, W. S. (1965). Multidimensional scaling of similarity. *Psychometrika*, *30*(4), 379–393.